Available online at www.sciencedirect.com
ScienceDirect
Journal of the European Ceramic Society 30 (2010) 1381–1389
www.elsevier.com/locate/jeurceramsoc

# Tailoring the microstructure of reaction-sintered alumina/lanthanum hexaaluminate particulate composites

Zahra Negahdari *, Monika Willert-Porada

*Chair of Materials Processing, Faculty of Engineering Science, University of Bayreuth, Universitatstr. 30, 95440 Bayreuth, Bavaria, Germany*

Received 5 March 2009; received in revised form 5 October 2009; accepted 20 October 2009
Available online 26 November 2009

**Abstract**

The aim of this study was modification of the microstructure and adjustment of the porosity in alumina/lanthanum hexaaluminate particulate composites, by altering the lanthanum hexaaluminate content, for the further development of new materials that can be applied in several technological processes. The amount of lanthanum hexaaluminate was varied from 2.8 to 80 vol.% in particulate composites. As a novel approach to develop homogenously distributed dense and porous alumina/lanthanum hexaaluminate particulate composites, a carbonate co-precipitation method was applied to produce lanthanum aluminate-coated alumina particles. For the coating process itself, a surface charge adjustment called 'electrostatic attraction' was utilised. Subsequent reactive sintering of the calcined-coated particles caused the in situ formation of lanthanum hexaaluminate platelets inside the alumina matrix. The prepared composite powders, as well as the sintered samples, were characterised by FE-SEM, TEM, XRD, dilatometry, and mercury porosimetry. The results revealed that the uniform distribution of the low amount of lanthanum hexaaluminate prohibited the grain growth of alumina matrix and resulted in denser microstructures, whereas the increase in the lanthanum hexaaluminate content yielded more porous microstructures.


*Keywords:* Composites; Microstructure-final; Porosity; $Al_2O_3$; Lanthanum hexaaluminate ($LaAl_{11}O_{18}$)

## 1. Introduction

Due to their light weight, high mechanical strength and fracture toughness, high temperature capabilities, low thermal expansion, high abrasive resistance, and graceful failure under loading, ceramic composites have attracted attention for the development of desired materials required for space, terrestrial, energetic, and many other applications.[1,2] To date, much effort has been spent on the advancement of non-oxide ceramic composites, but most of the superior mechanical properties of these composites can only be of benefit if they are used in inert atmospheres. Therefore, the possible breakthrough of oxide/oxide ceramic composites with long-time stability at high temperatures even in oxidising atmospheres have attracted much more attention recently.[3] The properties of oxide-based ceramic composites are strongly dependent on the microstructure characteristics, e.g., the size and shape of grains, the amount of porosity and the pore size, the distribution of pores in the body, and the nature and distribution of any second phases. Therefore, designing the microstructure via processing is an important key for obtaining the desired properties. From the processing point of view, there is a growing interest in the development of particulate composites with microstructures exhibiting plate-like morphologies,[4] as well as in porous composite ceramics with pore morphological and thermochemical stability and desired thermophysical properties for applications at elevated temperatures.[5]

Lanthanum hexaaluminate (LHA) with an ideal stoichiometry $LaAl_{11}O_{18}$, a magnetoplumbite/β-alumina structure, and a platelet-like morphology is a candidate material for adjustment of the fibre-matrix interfaces,[6] reinforcement of the particulate composites,[7] and then applications in high-temperature thermal barrier coatings.[8] The solid-state formation of LHA by the reaction between lanthanum aluminate ($LaAlO_3$) and α-alumina ($Al_2O_3$) is extremely slow and requires high temperatures.[9]

* Corresponding author. Tel.: +49 0921 557207; fax: +49 0921 557205.
*E-mail addresses:* z_negahdari@yahoo.com, zahra.negahdari@uni-bayreuth.de (Z. Negahdari).

0955-2219/$ – see front matter © 2009 Elsevier Ltd. All rights reserved.
doi:10.1016/j.jeurceramsoc.2009.10.010

The very slow formation of LHA, as well as the difficulties in homogeneously distributing the secondary LHA particles in the host matrix, have resulted in the in situ development of LHA platelets in an alumina matrix by a number of researchers. Jang and Kishi[10] fabricated dense alumina/LHA composites with compositions from 5 to 20 vol.% $LaAl_{11}O_{18}$ by the solid-state reaction between $La_2O_3$ and α-$Al_2O_3$ and hot-pressing above 1500 °C. Chen and Chen[7] could toughen alumina/LHA particulate composites by adding $La(NO_3)_3$ to the alumina powder and subsequently sintering above 1650 °C for 3 h. Barrera-Solano and Esquivias[11] studied the in situ formation of LHA in an alumina matrix as a function of preparation methods, including both a conventional solid-state reaction of commercial $Al_2O_3$ powder and $La(NO_3)_3$ as well as a sol–gel method starting with boehmite and $La(NO_3)_3$. In both cases, homogeneous distribution of the reinforcing phase was achieved. However, samples prepared by solid-state reaction densified more easily than those prepared via sol–gel, but the formation of the LHA phase occurred at a lower temperature in samples prepared by the sol–gel approach, preventing further sintering. Recently, Wu et al.[12] prepared $Al_2O_3$–25 vol.% LHA composites via a co-precipitation route using $La(NO_3)_3{\cdot}6H_2O$ and $Al(NO_3)_3{\cdot}9H_2O$ as starting materials in the presence of sintering aids like CAS ($CaO–Al_2O_3–SiO_2$) and $AlF_3$ at 1550 °C for 4 h. Despite all the mentioned efforts, optimisation of the green processing of alumina/LHA particulate composites, by decreasing the diffusion distance to lower the reaction temperature, is of great interest.

By increasing the LHA content in particulate ceramics, the low sinter-ability of LHA due to the suppressed interlayer diffusion of atoms[13] introduces porosity into the system. This fact can be utilised to overcome the yet unresolved problem in the development of LHA-based thermal barrier coatings, i.e., making adjustments of the microstructure (porosity) and composition along the thickness[14] in order to arrive at a material exhibiting low thermal conductivity combined with structural reliability and high stress tolerance. Therefore, studying the phase evolution and sintering behaviour of composite powders with higher LHA content are two main requirements for understanding and tailoring the microstructure development in alumina/LHA particulate composites.

In this study, in order to develop dense and porous $Al_2O_3$/LHA particulate composites with well-distributed LHA platelets and adjusted porosity, alumina particles were coated with lanthanum aluminate via an 'electrostatic technique' for in situ formation of a required amount of LHA by subsequent sintering. The sintering behaviour and tailored microstructures of the particulate composites were investigated as a function of LHA content. The results of this study developed new functional laminate materials, with a range of compositions, microstructures, and mechanical and thermal properties, that will be reported in future publications.

## 2. Experimental procedure

SG-A16 alumina (α-$Al_2O_3$, purity > 99.8%, particle size < 0.6 μm, Alcoa Industrial Chemicals, USA), as the starting material, was dispersed in distilled water. The solid content of suspension was 20 vol.%, and for better dispersion of alumina particles, 0.1 wt.% of ammonium polyacrylate ($NH_4^+$-PA, BYK-Chemie, Germany) was used as an anionic dispersant. The suspension was stirred by a magnetic stirrer for 5 min and subsequently sonicated for 15 min using a tip-ultrasonifier (Model 250&450, Branson Ultrasonic Corporation, USA) at "50% pulsed mode" for deagglomeration of alumina particles. For the preparation of $Al_2O_3$–$x$ vol.% LHA composite powders (where $x = 2.8$, 20, 40, 60, and 80), appropriate amounts of aluminium nitrate ($Al(NO_3)_3{\cdot}9H_2O$, from Fluka Co.) and lanthanum nitrate ($La(NO_3)_3{\cdot}6H_2O$, from Alfa Acer Co.) were dissolved in 200 ml distilled water and introduced to an alumina suspension according to Table 1.

Table 1
Notations and ingredients for each $Al_2O_3$–$x$ vol.% LHA composite's powders.

| Composite | Notation | Starting materials (g) | | |
|---|---|---|---|---|
| | | A16 | $Al(NO_3)_3{\cdot}9H_2O$ | $La(NO_3)_3{\cdot}6H_2O$ |
| Monolithic alumina | A | – | – | – |
| $Al_2O_3$–2.8 vol.% LHA | C2.8 | 35 | – | 0.594 |
| $Al_2O_3$–20 vol.% LHA | C20 | 35 | 4.01 | 4.626 |
| $Al_2O_3$–40 vol.% LHA | C40 | 35 | 8.62 | 13.07 |
| $Al_2O_3$–60 vol.% LHA | C60 | 35 | 13.91 | 21.085 |
| $Al_2O_3$–80 vol.% LHA | C80 | 35 | 20.07 | 30.41 |

For further preparation, the initial pH of suspensions was changed to 8–9 by dropwise addition of 0.2 M ammonium carbonate solution ($NH_4CO_3$, Merck Co.) as a precipitant agent while stirring vigorously. The products were collected by vacuum filtration and washed successively three times with distilled water and ethanol and subsequently dried at 60 °C for 24 h. For further processing into green parts, the dried powders were calcined at 850 °C for 3 h, and successively the calcined powders were ground using an agate mortar and passed through a 200 mesh sieve.

Thirty grams of each of the prepared composite powders as well as SG-A16 alumina were dispersed individually in 100 ml of an ethanol/water solution (2:l, v/v). The suspensions were stirred by a magnetic stirrer for 1 h while the temperature was kept at 50 °C. To improve formability of the dry ceramic powders, 4 wt.% of PVA ($M_w = 15{,}000$, Fluka) was individually dissolved in 50 ml distilled water at 70 °C and added to the suspensions while sonicating for 1 h. The slurries were partially dried by a rotary evaporator at 50 °C and subsequently dried completely at 60 °C for 10 h under vacuum.

For the cylinder-shaped monolithic samples (30 mm diameter, about 6 mm thickness), the prepared powders were sieved through a 100-μm screen and pressed at 300 MPa at room temperature using an uniaxial hydraulic press (P/O/Weber GmbH). After removal of organic binders at 800 °C for 3 h using a very slow heating/cooling rate, the green bodies were sintered in air (Nabertherm HT 08/17). Initially, the samples were heated at 8 °C/min to 1575 °C for 10 min and subsequently cooled back down to 1400 °C for 10 h. The samples were cooled down at 8 °C/min to room temperature.

The electrokinetic behaviour of alumina suspensions was investigated with an ultrasound spectrometer (DT-1200, Dispersion Technology Co., USA).

The density of the sintered samples was measured by a method based on Archimedes' principle. In order to investigate the open pore size distributions of the sintered composites, mercury porosimetry measurements were done with a Micromeritics, Autopore III porosimeter.

The X-ray diffraction (XRD) patterns were collected on a Philips Diffractometer PW 3040 using a Cu-Kα ($\lambda = 1.5418$ Å) radiation source with a nickel filter. JCPDS cards 46-1212, 05-0602, 39-0009, 31-0022, and 33-0699 were respectively used to identify α-$Al_2O_3$, $La_2O_3$, $La_{10}Al_4O_{21}$, $LaAlO_3$, and $LaAl_{11}O_{18}$.

For investigation of the sintering behaviour of different composites, the length change of the de-bindered samples was measured using a Netzsch, 402E/7 Dilatometer.

A field emission gun scanning electron microscope LEO 1530 (FE-SEM, Gemini) was used for microstructural characterisation. The cross-sectioned areas of the sintered samples were polished with 1-μm diamond paste and subsequently thermally etched at 1475 °C for 20 min. The samples were coated with a 2-nm thick layer of Pt/Pd by a Cressington sputter coater, 208 HR. Furthermore, a FE 200 field emission transition electron microscope (Zeiss Ltd., Germany) operating at an accelerating voltage of 200 kV was used for microstructural observations. The thin layers of the sintered samples were prepared by ion milling using a LEO 1540 Gimini focused ion beam microscope (FIB) at an accelerating voltage of 30 kV.

## 3. Results and discussion

### 3.1. Coating of alumina particles by lanthanum aluminate via electrostatic attraction

Fig. 1 shows the effect of ammonium polyacrylate (NHPA) addition on the electrokinetic behaviour of alumina particles. Due to the presence of attractive Van der Waals forces and the low surface charge on alumina particles at a pH around 7, the alumina particles were prone to agglomeration. In order to prevent defects in the microstructure caused by agglomeration after drying the powder, it was essential to prevent agglomerates from forming or eliminate them from the suspension prior to fabrication of the green body. The addition of anionic NHPA shifted the isoelectric point from ~9 to a value of ~4, and a significant negative charge was developed at natural pH (~−50 mV) that was high enough to disperse the alumina suspension. Therefore, the stability of the suspension improved because of the long-range repulsion resulting from electrostatic and steric interactions.[15]

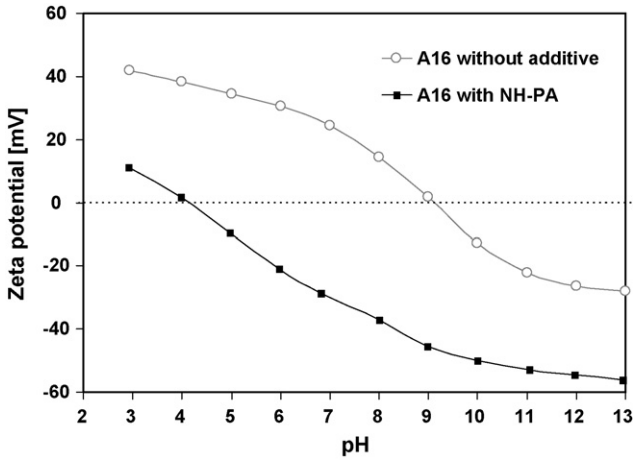


Fig. 1. Electroacoustic zeta potential dependence on pH for aqueous α-$Al_2O_3$ suspensions with and without the addition of dispersant.

Table 2
Phase evaluation of the C80 powder after heat treatment at different temperatures.

| Temperature (°C) | Phases detected by XRD |
|---|---|
| 850 | $Al_2O_3$, $La_2O_3$, $La_{10}Al_4O_{21}$, $LaAlO_3$, ... |
| 950 | $Al_2O_3$, $La_2O_3\downarrow$, $La_{10}Al_4O_{21}\downarrow$, $LaAlO_3\uparrow$ |
| 1050 | $Al_2O_3\downarrow$, $La_2O_3\downarrow$, $La_{10}Al_4O_{21}\downarrow$, $LaAlO_3\uparrow$ |
| 1150 | $Al_2O_3$, $LaAlO_3$ |
| 1250 | $Al_2O_3$, $LaAlO_3$ |
| 1500 | $Al_2O_3\downarrow$, $LaAl_{11}O_{18}$, $LaAlO_3$ (trace) |

In addition to the increase in surface charge of the alumina particles yielding better stabilisation of the suspension, the addition of NHPA could also facilitate the homogenous deposition of smaller La- and Al-containing compounds during the co-precipitation of lanthanum aluminate on the alumina particles. As is shown schematically in Fig. 2, the utilisation of ammonium polyacrylate to induce a negative charge on the surface of alumina particles in the pH range of 7–9 enhanced the attraction of the positively charged metal ions on the surface of the α-$Al_2O_3$ particles.

Due to the attraction of cations on the surface of the alumina particles, when the critical solute concentration for heterogeneous nucleation is reached, lanthanum and aluminium compounds nucleate on the surface of the alumina particles. The coating evolution is supposed to be accomplished by growing the nuclei to form a somewhat uniform coating.

### 3.2. Morphology and phase evolution of composite powders

The XRD results of the C80 powder calcined at different temperatures for 3 h are shown in Table 2. According to the XRD results, it can be concluded that the observed bright phases in the backscattered-SEM image (BSE) of C80 powder calcined at 850 °C (Fig. 3a) were lanthanum-containing compounds like $LaAlO_3$, $La_{10}Al_4O_{21}$, and $La_2O_3$. Fig. 4a demonstrates the TEM micrograph of C80 powder after calcinations at 850 °C. The figure shows that the smooth surface of the alumina particles was partially decorated with a fluffy thin coating of nanocrystalline structure that was supposed to be $La_{10}Al_4O_{21}$, due to the lower amount of La in the EDS result, and that some areas had $La_2O_3$ and $LaAlO_3$. The EDS analysis clarified that the coating composition consisted of Al, La, and oxygen (Fig. 4b).

The XRD results confirm that calcination at 850 °C was not sufficient for full formation of $LaAlO_3$. This means that, due to different hydrolysis rates, the co-precipitation technique produced an intimate mixture of precipitates, such that there

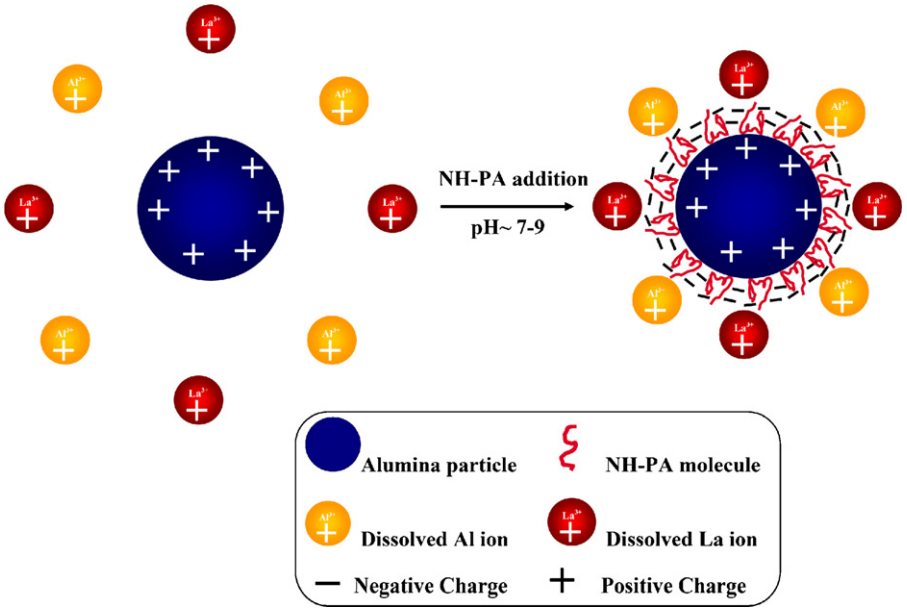


Fig. 2. Schematic drawing of the cation attraction on α-alumina particles by electrostatic interactions.

was a need for further heat treatment that could be obtained while sintering. Although $La_{10}Al_4O_{21}$ and $La_2O_3$ phases were present in the composite powder up to 1050 °C, their intensities decreased continuously with increasing temperatures. At temperatures higher than 1150 °C, the other phases, except alumina and $LaAlO_3$, vanished. Microscopic observations of the heat-treated C80 powder at 1250 °C (Fig. 3b) in comparison with the calcined powder at 850 °C declare that, by increasing temperature, fine $LaAlO_3$ particles sized smaller than 100 nm homogeneously surround alumina particles and provide a well distribution of lanthanum-containing compounds around them for further solid-state reaction to produce lanthanum hexaaluminate.

### 3.3. Sintering behaviour of lanthanum aluminate-coated alumina powders

The sintering behaviour of alumina and alumina/LHA composite powders was studied by dilatometry. The results (Fig. 5) reveal that the $Al_2O_3$ compact commenced shrinking

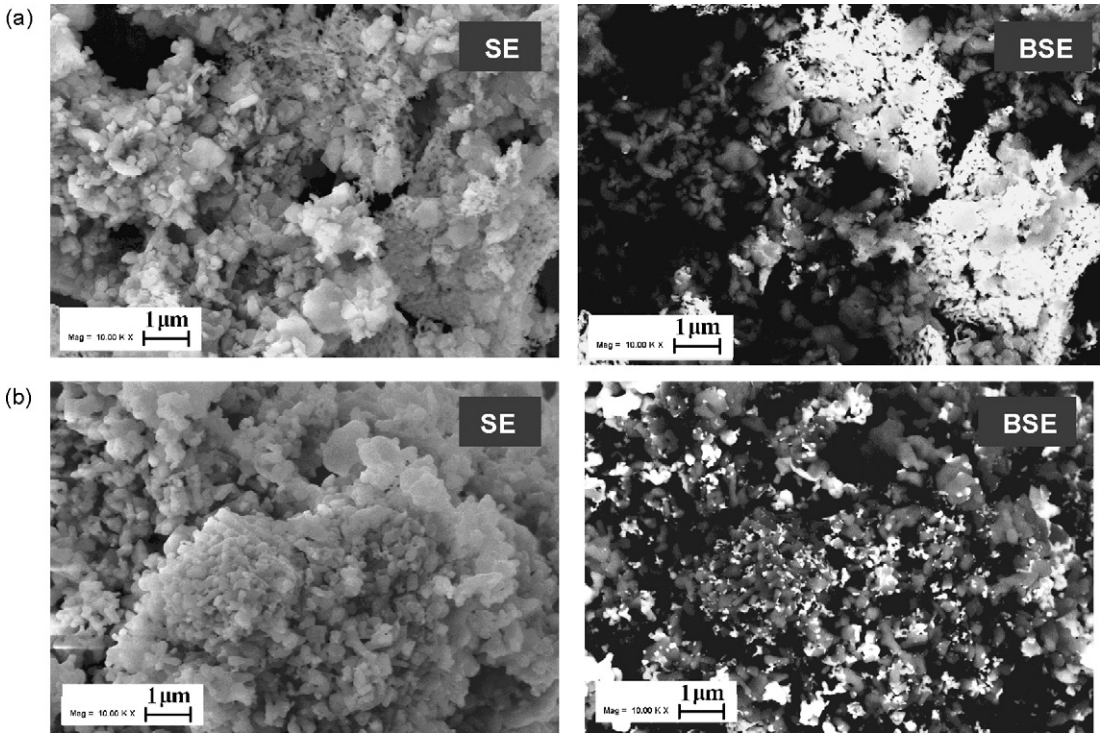


Fig. 3. FE-SEM micrographs of the C80 powder calcined at 850 (a) and 1250 °C (b) for 3 h.

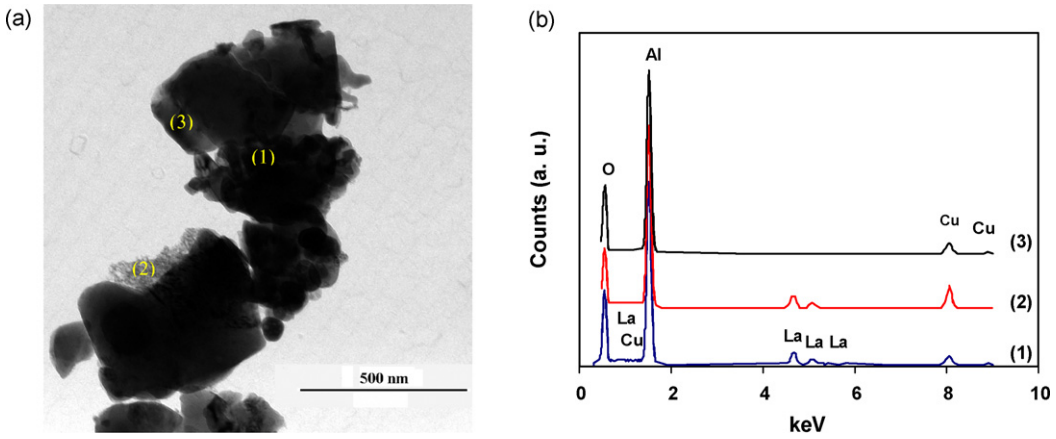


Fig. 4. Bright-field TEM image (a) and EDS analysis (b) of lanthanum aluminium oxide-coated alumina particles after heat treatment at 850 °C.

at ~1150 °C. In comparison with alumina, alumina/LHA composites commenced to sinter with a slightly higher shrinkage rate and at a higher temperature of approximately 1300 °C. The final shrinkage was in the range from 8 to 16% obtained at 1500 °C for 2.8–80 volume fractions of LHA. This implies that the LHA formation delayed the initiation of densification and sintering regardless of the volume fraction of lanthanum hexaaluminate, in contrast to the maximum sintering shrinkage that was affected by the volume fraction of LHA. A similar delay in the initial temperature of sintering for alumina/calcium hexaaluminate particulate composites has been also observed.[16] After dwelling at 1500 °C for 2 h, the final shrinkages of 16.3 and 16.1% for composites containing 2.8 and 20 vol.% LHA, respectively, are nearly the same amount lower than the 17.8% shrinkage of the pure alumina sample. It can be concluded that the sintering behaviour of the alumina matrix is more dominant in composites with less than 20 vol.% LHA content. By increasing the volume fraction of LHA, the sintering behaviour of the LHA compound governs the densification of the composites. The comparable final shrinkages and densification behaviour of 60 and 80 vol.% LHA composite ceramics imply that LHA-rich composites have low sinter-ability.

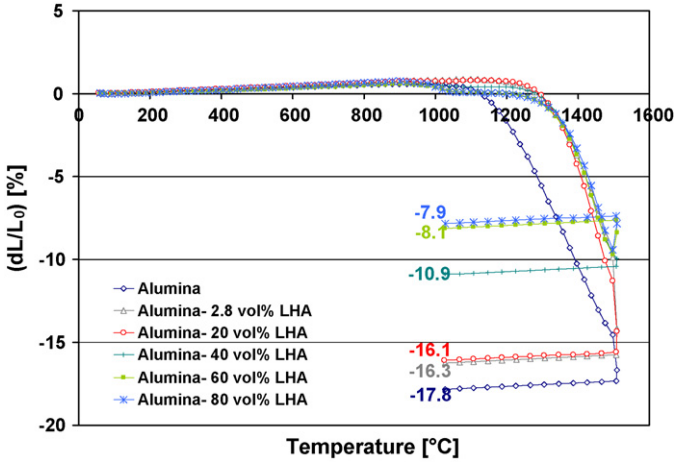


Fig. 5. Comparison of the linear shrinkage curves for alumina and alumina/LHA composite ceramics.

The dilatometry results also help to illuminate the reactivity and sinter-ability of the composite powders. The BET-specific surface area of calcined composite powders at 850 °C (Table 3) increased with increases in the volume fraction of LHA, which is due to the formation of La-containing second phases of finer particle size around and in between the alumina particles.

According to the Herring's scaling laws, with decreases in the particle size, both the rate of reaction and the rate of densification are enhanced.[17,18] The rate of LHA formation through the solid-state reaction on the surface of the alumina particles will vary with particle size, $G$, in accordance with $G^{-1}$ or $G^{-2}$, while the densification rate of composite powders will vary as $G^{-3}$ or $G^{-4}$. Therefore, increasing the amount of fine particles enhanced the solid-state reaction to a larger extent. The first shrinkage step for alumina–$x$ vol.% LHA ($x \geq 40$) prior to sintering can be interpreted as the formation of lanthanum aluminate ($LaAlO_3$) from non-reacted alumina and lanthanum-rich compounds, starting at almost 950 °C and smoothly going to completion. As temperature is increased, the $LaAlO_3$ engages in further reactions to form LHA. Comparing the theoretical density of LHA in composites with the density of the reacting species $Al_2O_3$ and $LaAlO_3$, it becomes evident that, upon complete formation of LHA in samples, a volume expansion is expected (Fig. 6). Therefore, as the temperature is raised to 1500 °C and the samples are held at this temperature for 2 h, the formation reaction of LHA from $Al_2O_3$ and $LaAlO_3$ is completed. This reaction is responsible for the final expansion in the dilatometry curves. Specifically, by dwelling at 1500 °C for 2 h, the dimensional change is reversed as the expansion due to reaction becomes predominant. The plate-like morphology of the LHA grains could also contribute to an overall expansion, because of the thermal expansion anisotropy of the platelets. It is expected that, after the completion of LHA formation,composites

Table 3
BET-specific surface area of alumina and alumina/LHA powders calcined at 850 °C.

| Composite | A | C2.8 | C20 | C40 | C60 | C80 |
|---|---|---|---|---|---|---|
| BET ($m^2\ g^{-1}$) | 7.1 | 7.94 | 8.89 | 10.73 | 13.63 | 13.83 |

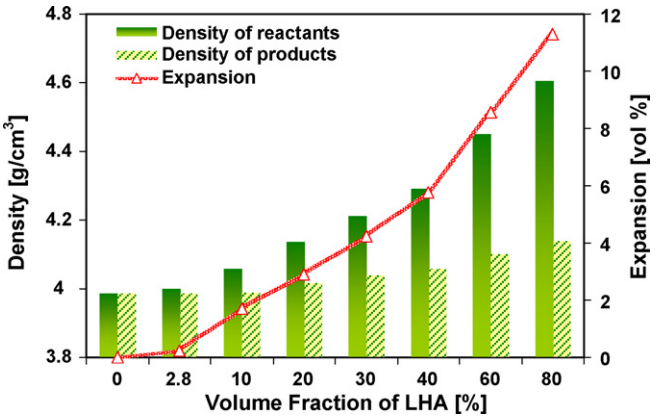


Fig. 6. The calculated volume expansion of different composites after the completion of LHA formation, according to the differences between the theoretical densities of the reactants and products ($Al_2O_3$: 3.985 g/cm$^3$, $LaAlO_3$: 6.17 g/cm$^3$, $LaAl_{11}O_{18}$: 4.17 g/cm$^3$).

will start to densify and shrink upon further increasing temperature.

### 3.4. Effect of lanthanum hexaaluminate content on the microstructure of sintered alumina/LHA particulate composites

The variation of relative density versus LHA content for reaction-sintered alumina/LHA composites is tabulated in Table 4. The density obtained for all alumina/LHA composites after sintering was no higher than the density of monolithic alumina (~97%). Additionally, the relative density of the composites decreased from 96 to 65% by increasing the LHA content from 2.8 to 80 vol.%. This demonstrates that the in situ formation of LHA led to retardation of the densification rate. The main reason for this phenomenon is attributed to the low sinter-ability of LHA with a platelet structure.

The FE-SEM micrographs of alumina and alumina/LHA particulate composites are compared in Fig. 7 according to LHA content. In the SE-images the pore distribution and the grain structure are visualised with increasing LHA volume fractions, whereas the BSE images reveal the size, shape, and distribution of the LHA grains within an alumina matrix depending upon the LHA content. By increasing the volume fraction of LHA, the increase in the content of elongated LHA particles is visible as the bright contrast distributed in the dark contrast of the fine equiaxed alumina matrix.

Monolithic alumina exhibits a microstructure with a typical bi-modal grain size distribution (Fig. 7a). Remarkably, in the 2.8 vol.% LHA composite ceramic C2.8 (Fig. 7b), the alumina matrix has a finer grain size distribution as compared to the monolithic alumina. It has a homogenous microstructure that is composed of very fine equiaxed-grained alumina matrix (1–2 μm in size) and well-distributed plate-like LHA grains. The LHA grains are located largely at triple grain junctions and are significantly smaller than the alumina grains.

Table 4
The relative density of reaction-sintered alumina/LHA composite ceramics.

| | LHA content (vol.%) | | | | | |
|---|---|---|---|---|---|---|
| | 0 | 2.8 | 20 | 40 | 60 | 80 |
| Relative density (TD %) | 97 | 96 | 90 | 79 | 72 | 65 |

The grain growth suppression of alumina results from the pining of the grain boundaries by LHA platelets as well as the effect of $La^{3+}$ dopant. In polycrystalline materials, small grains have a tendency to shrink and large grains have a tendency to grow by the Ostwald ripening process. The Zener stress, produced by interaction between the migrating grain boundaries and dispersed LHA particles, acts as a friction that opposes both movements and retards grain growth. Since the grain size of the alumina matrix is less than 10 μm, grain boundary diffusion dominates the densification rate and grain growth. $La^{3+}$ cation segregation at grain boundaries suppresses the grain boundary diffusivity by increasing the ionic bonding strength between Al and O ions at the grain boundaries.[19]

With increases in LHA content (Fig. 7c–f), the grain size distribution of the alumina matrix remains uni-modal but shifts to smaller grain sizes, whereas the grain size and aspect ratio of the LHA platelets increase. High-aspect ratio LHA platelets exert much higher forces on grain boundaries.[20] In addition, the porosity that increases by rises in the LHA content (Fig. 8) prevents grain growth of the fine alumina matrix by Zener pining. Therefore, composites containing higher amounts of LHA have smaller grain sizes (less than ~1 μm) as compared with monolithic alumina, in which the average grain size is larger than 2 μm. Finally, it can be concluded that the optimisation of green processing and an improved distribution of LHA grains in the matrix contribute to the development of a quite uniform microstructure. The scatters of the relative magnitudes of the surface energies and the diffusional grain growth processes are reduced; therefore, grain growth on specific surfaces and abnormal grain growth do not occur, unless higher sintering temperature are applied in order to achieve higher densities.

As shown in Fig. 8, the sintered alumina and the alumina/LHA particulate composite with LHA content less than 20 vol.% contain meso-pores with an average pore size smaller than ~20 nm. By increasing the LHA content to 20 vol.%, the grain size of the alumina matrix decreases and uni-modal pore size distribution of the composites changes to bi-modal with the average pore size of ~50 nm observed between the grains. Using SEM, these pores are found to be intergranular. Further increases in LHA content (≥40 vol.%) of plate-like structure shifts the pore size distribution of the composites to larger open pores with an average size of ~0.2 μm. Alumina/80 vol.% LHA with 35% open-porosity is the most porous ceramic among these composite materials, and it has pores homogenously distributed in the LHA matrix.

Chen and Chen[7] were able to achieve dense particulate composites with higher LHA contents, but this study, in comparison, has plate-like LHA grains with lower aspect ratios and larger grain sizes. In contrast with the work of Jang and Kishi[10], this work shows alumina/LHA ceramics fabricated by pressureless sintering at a temperature lower than 1575 °C and alumina-rich composites with $Al_2O_3$ grains of a relatively

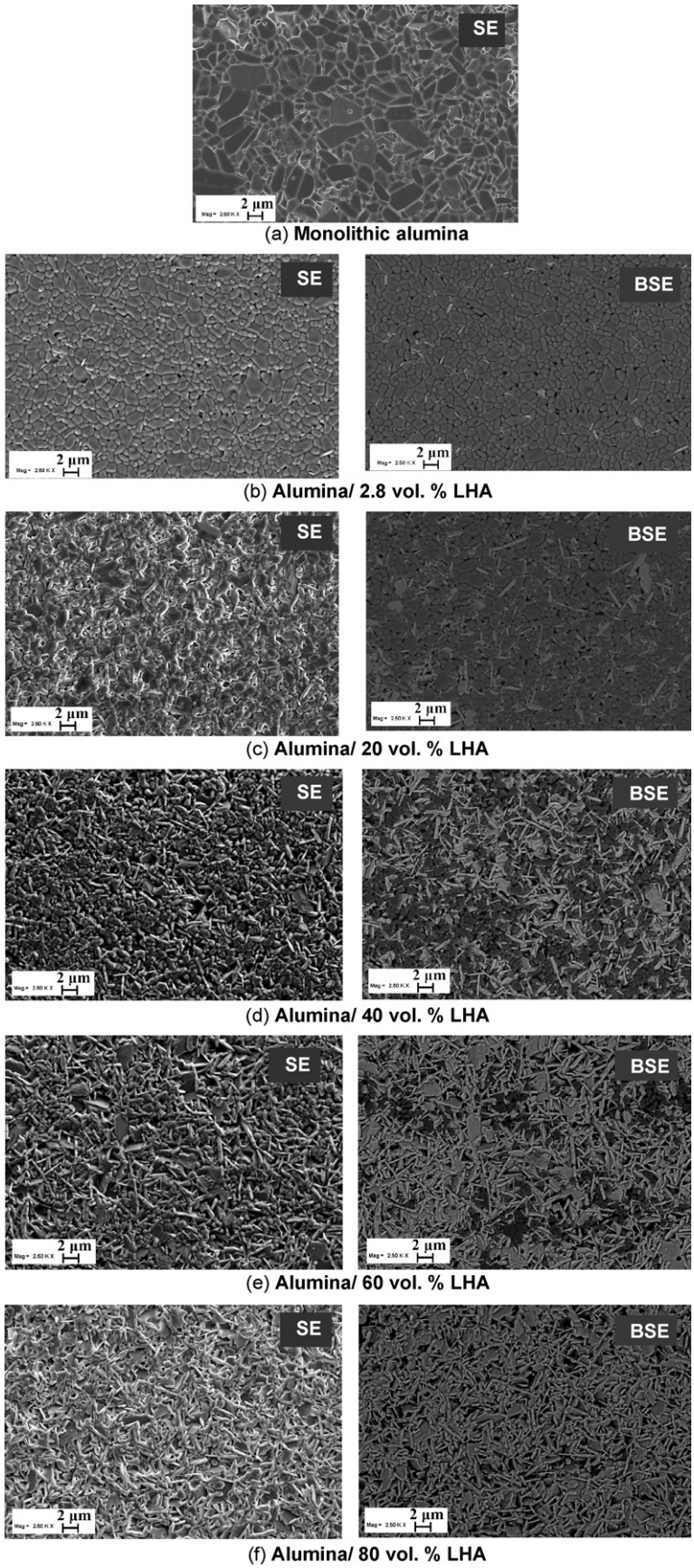


Fig. 7. FE-SEM micrographs of microstructures of (a) monolithic alumina and (b–f) alumina/LHA composite ceramics after sintering at 1575 °C/10 min-1400 °C/10 h.

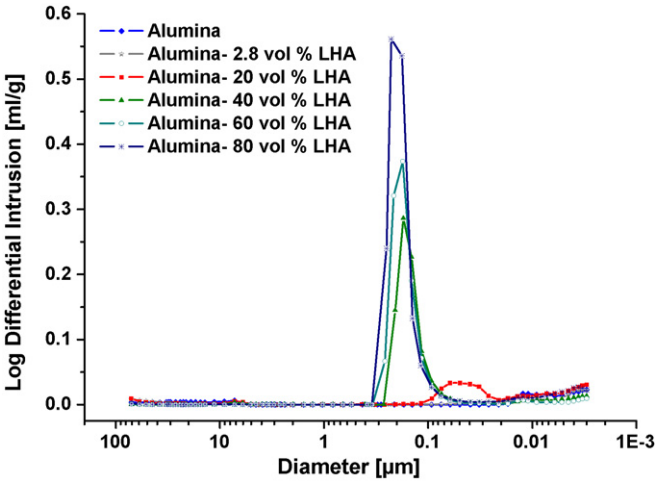


Fig. 8. Comparison of the pore size distribution for sintered alumina and alumina/LHA composite ceramics as a function of lanthanum hexaaluminate content.

smaller grain size (less than 2 μm). This can be attributed to the two-stage sintering at lower temperatures and enhanced homogenous distribution of LHA platelets inside the matrix by an electrostatic attraction method. Highly similar to the work of Barrera-Solano and Esquivias,[11] increases in the LHA content to more than 20 vol.% yielded no noticeable densification. It should be noted that only reports using sintering aids like $SiO_2$ and CAS ($CaO{\cdot}Al_2O_3{\cdot}SiO_2$) have achieved higher densities for sintered composites with a 20 vol.% at temperatures higher than 1550 °C.[12]

The microstructures of the sintered alumina/lanthanum hexaaluminate particulate composite are in clear contrast with those observed by Vishista et al.[21] and An et al.[22] in alumina/calcium hexaaluminate composites, in which the grain size distribution of the alumina matrix shifts to the coarser grain sizes by the addition of platelet calcium hexaaluminate. The presence of liquid forming dopants can be considered as the main reason for normal

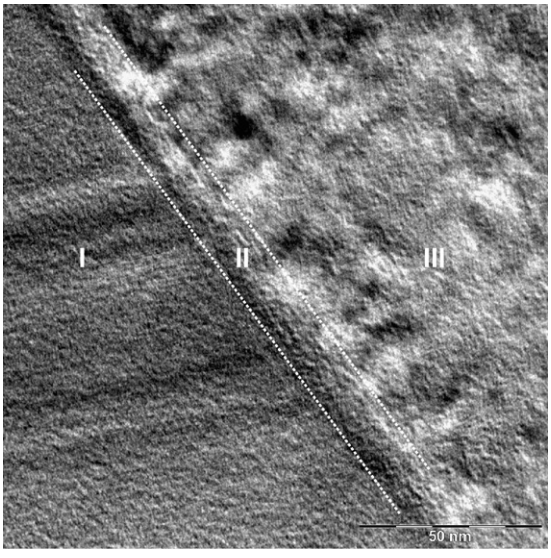


Fig. 9. HR-TEM micrograph of a grain boundary region in the sintered alumina/20 vol.% LHA composite ceramic.

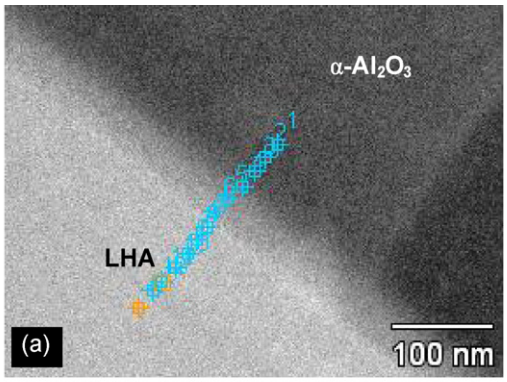


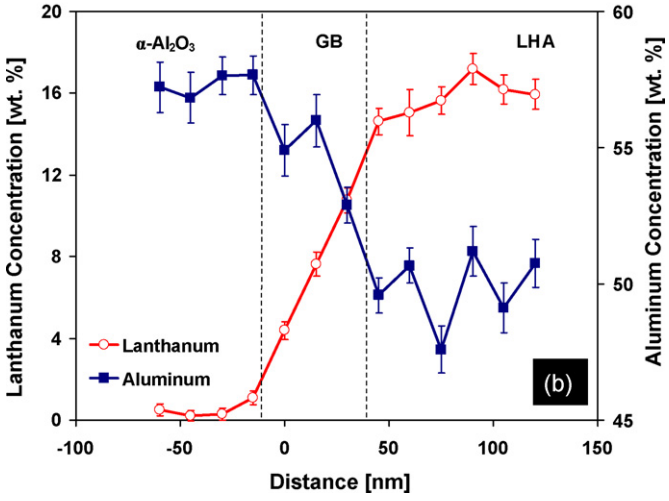


Fig. 10. STEM image obtained for the grain boundaries in the $Al_2O_3$/20 vol.% LHA composite ceramic (a) and EDS from the grain boundary into the grain interior (b) (electron probe size of 2 nm).

and abnormal grain growth in alumina/calcium hexaaluminate particulate composites. As observed in Fig. 9, the transmission electron microscopy showed that no amorphous or liquid phase exists in the grain boundaries of the alumina and LHA grains, but three regions of different morphologies are identified in the alumina/LHA grain boundaries, labelled as I–III. Regions I and III were ascribed to α-$Al_2O_3$ and LHA. The chemical composition profiles obtained by EDS (Fig. 10) analysis indicate that the second regions of ∼10 nm thickness is the reaction interface between α-alumina and LHA with a gradient in chemical composition. The parabolic lanthanum concentration gradient across the interface layer is attributed to diffusion controlled reaction formation, which provides the driving force for further lanthanum diffusion through interfaces.[23]

## 4. Conclusion

LHA (2.8–80 vol.%) was homogeneously distributed in an alumina matrix by the in situ reaction of carbonate co-precipitated lanthanum aluminium oxide coating on alumina particles. Subsequently, the sintering behaviour and microstructure of the reaction-sintered composite ceramics were studied. Independent of the LHA content level, LHA delayed the initiation of bulk shrinkage of the composite ceramics from 1150

to 1300 °C. In composites with less than 20 vol.% LHA content, the sintering behaviour of the alumina matrix was more dominant, but by increasing the volume fraction of LHA, the sintering behaviour of the LHA compound governed the densification and final shrinkage of the samples. By increasing the amount of LHA in the samples (esp. for volume fractions over 40%), the increase in the volume fraction of fine co-precipitated particles enhanced the densification stronger than the LHA formation reaction. However, by dwelling at 1500 °C for 2 h, the dimensional change was reversed as the expansion of the LHA formation reaction became predominant.

A density higher than the density of monolithic alumina (∼97%) was not obtained for any alumina/LHA composite ceramics. Plate-like LHA grains could also reduce grain growth to a greater extent by introducing porosity into the system. Therefore, composite ceramics containing more LHA had an alumina matrix with a uni-modal grain size distribution and smaller grain sizes (less than ∼1 μm) compared with monolithic alumina, in which there is a bi-modal grain size distribution and an average grain size larger than 2 μm. Alumina/LHA particulate composites with LHA contents less than 20 vol.% had meso-pores with an average pore size smaller than ∼20 nm. By increasing the LHA content to 20 vol.%, the uni-modal pore size distribution of the composite ceramics changes to bi-modal with an average pore size of ∼50 nm. Larger increases in LHA content (≥40 vol.%) shifted the pore size distribution of the composite ceramics to larger open pores with an average size of ∼0.2 μm and increased porosity.

## Acknowledgments

The financial support of the Bavarian Science Foundation within the doctoral grant DPA-52/05 is gratefully acknowledged. In addition, the first author would like to thank Prof. Dr. Walter Krenkel, Dr. Ali Saberi, Mr. Sven Scheler, Mrs. Elisa Guimaraens, Mr. Christian Liebscher, and Mr. Benjamin Gossler from University of Bayreuth for their great technical support.

## References

1. Bansal NP. *Handbook of Ceramic Composites*. Kluwer Academic Publishers; 2005.
2. Krenkel W, Naslain R, Schneider H. *High Temperature Ceramic Matrix Composite*. Wiley-VCH; 2001.
3. Wendorff J, Janssen R, Clauss N. Model experiments on pure oxide composites. *Mater Sci Eng A* 1998;**250**:186–93.
4. Becher PF. Microstructural design of toughened ceramics. *J Am Ceram Soc* 1991;**74**(2):255–69.
5. Inagaki Y, Kondo N, Ohji T. High performance porous silicon nitrides. *J Eur Ceram Soc* 2002;**22**:2489–94.
6. Cinibulk MK. Hexaaluminates as a cleavable fibre-matrix interphase: synthesis, texture development, and phase compatibility. *J Eur Ceram Soc* 2000;**20**:569–82.
7. Chen PL, Chen IW. In-situ alumina/aluminate platelet composites. *J Am Ceram Soc* 1992;**75**(9):2610–2.
8. Gadow R, Lischka M. Lanthanum hexaluminate-novel thermal barrier coatings for gas turbine applications: materials and process development. *Surf Coat Technol* 2002;**151-2**:392–9.
9. Ropp RC, Carroll B. Solid-state kinetics of $LaAl_{11}O_{18}$. *J Am Ceram Soc* 1980;**63**(7–8):416–9.
10. Jang BK, Kishi T. Fabrication and microstructure of $Al_2O_3$ matrix composites by in-situ reaction in the $Al_2O_3$–$La_2O_3$ system. *J Ceram Soc Jpn* 1998;**106**(8):739–43.
11. Barrera-Solano C, Esquivias L. Effect of preparation conditions on phase formation, densification, and microstructure evolution in La-β-$Al_2O_3$/$Al_2O_3$ composites. *J Am Ceram Soc* 1999;**82**(5):1318–24.
12. Wu YQ, Zhag YF, Huang XX, Li BS, Guo JK. Preparation, sintering and fracture behaviour of $Al_2O_3$–$LaAl_{11}O_{18}$ ceramic composites. *J Mater Sci* 2001;**36**:4195–9.
13. Nair J, Nair P, Doesburg EBM, Van Ommen JG, Burggraaf AJ, Mizukami F. Textural stability as a characterisation tool of high temperature catalysts. *Mater Res Innov* 1998;**2**:72–8.
14. Cao XQ, Zhang YF, Zhang JF, Zhong XH, Wang Y, Ma HM, Xu ZH, He LM, Lu F. Failure of the plasma-sprayed coating of lanthanum hexaluminate. *J Eur Ceram Soc* 2008;**28**(10):1979–86.
15. Rahaman MN. *Ceramic Processing*. 1st ed. Taylor & Francis Group; 2008.
16. Asmi D, Low IM. Self-reinforced Ca-hexaluminate/alumina composites with graded microstructures. *Ceram Int* 2008;**34**(2):311–6.
17. Rahaman MN. *Sintering of Ceramic*. 1st ed. Taylor & Francis Group; 2008.
18. Herring C. Effect of change of scale on sintering phenomena. *J Appl Phys* 1950;**21**:301–3.
19. Yoshida H, Hashimoto S, Yamamoto T. Dopant effect on grain boundary diffusivity in polycrystalline alumina. *Acta Mater* 2005;**53**:433–40.
20. Hazzledine PM. Grain boundary pinning in two-phase materials. *Czech J Phys B* 1988;**38**:431–43.
21. Vishista K, Awaji H, Gnanam FD. Sol–gel synthesis and characterization of alumina-calcium hexaluminate composites. *J Am Ceram Soc* 2005;**88**(5):1175–9.
22. An L, Chan HM, Soni KK. Control of Calcium hexaluminate grain morphology in in-situ toughened ceramic composites. *J Mater Sci* 1996;**31**:3223–9.
23. Kingery WD. *Introduction to Ceramics*. John Wiley & Sons; 1960.